Hindawi
Journal of Chemistry
Volume 2022, Article ID 4917604, 13 pages
https://doi.org/10.1155/2022/4917604

Research Article

Green Synthesis of Hydroxyapatite Nanoparticles Using *Monoon longifolium* Leaf Extract for Removal of Fluoride from Aqueous Solution

Dawit Darcha Ganta,[1] **Belete Yilma Hirpaye**,[1] **Sabu Kuzhunellil Raghavanpillai**,[1] **and Solomon Yayeh Menber**[2]

[1]*Department of Applied Chemistry, Arba Minch University, Arba Minch, Ethiopia*
[2]*Department of Applied Chemistry, Mizan Tepi University, Tepi, Ethiopia*

Correspondence should be addressed to Dawit Darcha Ganta; devdarcha143@gmail.com

Received 26 October 2022; Revised 9 December 2022; Accepted 12 December 2022; Published 23 December 2022

Academic Editor: Jae Ryang Hahn

Hydroxyapatite ($Ca_{10}(PO_4)_6(OH)_2$) calcium phosphate is a robust and viable magnetic material for the treatment of polluted air, water, and soil. Because of its unique structure and appealing properties such as high adsorption capabilities, acid-base adaptability, ion-exchange capability, and thermal stability, hydroxyapatite (HAp) has a lot of potential in the field of environmental management. An aqueous extract of *Monoon longifolium* leaves was used for the preparation of hydroxyapatite nonparticles as the adsorbent for fluoride ion removal from aqueous solution in this work, resulting in bio-based hydroxyapatite nanoparticles. The prepared adsorbent was characterized by using instrumental techniques such as TGA/DTA, XRD, AAS, FT-IR, and UV-Vis spectroscopy as well as SEM. The batch adsorption approach was used to determine the optimum adsorption efficiency of HAp NPs under various experimental conditions. As a result, the best removal efficiency corresponds to 0.75 g HAp NPs, 15 mg/L, and pH 7 at 50 minutes (96%). The equilibrium adsorption data were better fitted into the Freundlich isotherms ($R^2 = 0.99$), and the pseudo-second-order kinetic model was found to be suitable ($R^2 = 0.99$) for the kinetic model. Fluoride ion adsorption on HAp NPs is spontaneous, endothermic, and possible at temperatures over 318 K, according to thermodynamic calculations. The results hint at a conclusion that the synthesized HAp NPs were an efficient adsorbent for the removal of fluoride ions and the overall process can be an economical choice for scaled-up water treatment processes.

1. Introduction

Water is one of the most necessary components for all kinds of life and essential in maintaining biodiversity on the planet. Every human being has a basic need for daily consumption. Pure water is scarce and hard to get. Water can be contaminated by natural sources or industrial effluents. One of these contaminants is fluoride ions derived from various sources. Fluorite (CaF_2), cryolite (Na_3AlFPO_6), and fluoroapatite ($Ca_5(PO_4)_3F$) are all found along with groundwater [1, 2]. Fluoride ion levels in drinking water that are too high have become a major topic of worry across the globe, causing serious health hazards. Excess fluoride consumption has been linked to the development of fluorosis, changes in DNA structure, a decrease in brain function in children, and even death when the dosage reach dangerously high levels [3]. As a result, lowering the fluoride ions levels in contaminated drinking water to a safer extent is a topic of research priority.

Fluoride ions can be removed from aqueous solutions using a variety of techniques. Due to their effectiveness, convenience, simplicity of design, ease of work up, and operation, adsorption-related techniques is more cost-effective and environmentally benign [4]. Several locally available and naturally occurring adsorbent materials, such as the most common activated alumina, activated carbon, activated clay, ceramic materials, bleaching earth,

diatomaceous earth, and carbonaceous materials produced from coffee grounds, have recently been tried in the context of identifying efficient and economical defluoridating agents [4–6].

However, the applicability of these adsorbents is limited, particularly in rural places in underdeveloped nations, due to their low efficiency, high production cost, and technical problems, as well as disposal issues. For these reasons, a considerable number of studies have dealt with various types of other absorbent materials. As a result, a significant number of studies on a variety of new absorbent materials have been carried out. Because of their chemical closeness to human bone and teeth, lack of secondary pollution, ease of supply, and strong defluoridation capacity, synthetic HAp NPs remain a leading candidate [7–10].

Hydroxyapatite is a bioceramic substance that is chemically related to human bones and hard tissues [11]. The most frequent crystal structure of hydroxyapatite is hexagonal, which belongs to the P63/m space group and has lattice parameters of $a = b = 9.432$ and $c = 6.881$ [12]. There is two types of Ca sites: the first has nine oxygen atoms and forms a polyhedron, while the second has five oxygen atoms and one hydroxyl group and forms an octahedron. Hydroxyl ions are present in columns perpendicular to the plane at the corners at regular intervals. Phosphate groups are present on the hexagonal exterior, and HAp is stable due to its unique tetrahedral structure [13]. The net positive charge of HAp NPs allows for the adsorption of negatively charged fluoride ions.

Currently, HAp NPs play a significant role in the environmental remediation effort. It can remove several contaminants such as Cu^{2+}, Pb^{2+}, Cd^{2+}, Co^{2+}, and Ni^{2+} as well as NO^{3-}, PO_4^{3-}, F^-, phenol, nitrobenzene, and Congo red because of its large surface area, excellent adsorption capacity, easy availability, less toxicity, and enhanced efficiency [14, 15]. As a result, the utilization of HAp NPs as an adsorbent in wastewater treatment can be termed a suitable and acceptable solution.

Due to their small pores and delayed diffusion process, HAp NPs have a limited capacity for storing larger molecules [16]. Controlling the particle size of HAp NPs during synthesis has always been a hurdle for the end user and the particles are prevented from agglomeration. Agglomeration usually causes a reduction in surface energy and is a favored phenomenon. The creation of core-shell type surface-functionalized HAp NPs has attracted a lot of attention since the polymer shell inhibits the agglomeration NPs and increases their stability [17–20]. The usage of bioextracts as a polymer matrix improves the efficient function of nanoparticles and environmental safety. For example, *Monoon longifolium (M. longifolium)* leaf extract has acidic functional groups that aid in cationic fluoride ion removal; the plant is also widely available in Ethiopia's tropical zones. Meanwhile, employing extracts of various parts of different plants as a capping agent in nanoparticle production could be a viable strategy to improve adsorption efficiency, suspension in a particular medium dispersion stability, structural variety, thermal stability, and recovery after use [21, 22].

In this research, we looked into a simple and eco-friendly method for generating HAp NPs using *M. longifolium* leaf extract. *M. longifolium* was used to convert calcium ions into nanoparticles without agglomeration and provide suitable functionality. X-ray diffraction (XRD), UV-visible spectroscopy (UV-Vis), Fourier transform-infrared (FT-IR) spectroscopy, and scanning electron microscopy (SEM) were used to investigate the surface morphology, structure, and adsorption properties of HAp NPs. The adsorption ability of HAp NPs for fluoride ion removal from synthetic water was tested under various conditions (pH, contact time, and adsorbent/adsorbate ratio, and dosage). To learn more about the occurrences during the processes of adsorption, researchers used adsorption kinetic, thermodynamics, and isotherm models.

2. Materials and Methods

Without any refining, the following chemicals and substances of analytical grade were used: $CaCl_2.2H_2O$ (Blux lab), H_3PO_4 (labol cheme), HCl (Sigma Aldrich), and NaF (Sigma Aldrich). To make synthetic solutions of fluoride ion, as a blank and also, for sample dilution, and other purification purposes, ultra-pureMilli-Q water was employed. To sonicate all of the glassware, a 5% HCl solution was employed, followed by rinsing with Milli-Q water.

2.1. HAp Nanoparticle Synthesis. After finding the optimum synthesis parameters, HAp NPs were synthesized using *M. longifolium* leaf extracts through the green process as follows. A solution of 0.6 M orthophosphoric acid (H_3PO_4) was also prepared and combined with the calcium chloride solution. After that, the *M. longifolium* leaf extract was added to the aforementioned mixture and agitated for 1 hour; NH_4OH was gradually added until the pH reached 10. This combination was constantly agitated for 3 hours, resulting in the formation of a colloidal solution. To allow the water to slowly evaporate, the solution was heated in a hot air oven at 45°C for 24 hours. The drying process was continued at 125°C for 12 hours to remove the leftover water, resulting in a yellowish, brittle, and porous dry substance. Finally, the dry product was calcined in a muffle furnace for 3 hours at 800°C, resulting in ultra-fine HAp NPs [23–25].

2.2. Characterization. A UV-visible spectrometer was used to record the absorption spectra (SCOROD-50, Germany). Powder samples of HAp NPs were carefully mixed with KBr powder and squeezed into thin transparent pellets for recording FT-IR spectra, which were done on a Perkin Elmer Spectrum 65 Spectrometer. D8 Advanced BRUKER AXS GmbH, Germany, was used to obtain the XRD patterns. Cuk radiation was used at a scan rate of 0.02/s (1.5406 A0, 45 kV, 40 mA). A scanning electron microscope was used to investigate the surface morphologies (JEOL-JSM6610 LV).

2.3. Fluoride Adsorption Study. The aquatic contaminant, sodium fluoride, was chosen as the model adsorbent. The tests were carried out in 250 mL Erlenmeyer flasks with

100 mL of the test solution in each flask. The pH of the proposed solution was adjusted using 0.1 M NaOH or HCl. The highest adsorption performance of the HAp NPs was determined by means of the batch fluoride ion sorption technique, by modifying the required contact time, temperature, initial fluoride concentration, adsorbent dosage, and pH. Adsorption kinetics was studied by obtaining samples from equilibrium solutions in Erlenmeyer flasks at various time intervals. An ion-selective electrode (ISE) directly attached to a potentiometer was used to determine the fluoride ion content in the supernatant. All experiments were performed in triplicate, and mean values are reported. All measurements were made at room temperature. The adsorption capacity and removal efficiency were calculated using

$$q = \frac{v(C_o - C_t)}{m} \times 100, \quad (1)$$

$$\text{revival efficiency} = \frac{C_o - C_e}{C_o} \times 100, \quad (2)$$

where v denotes the volume of the solution (L), m is the mass of the adsorbent (g), and C_o, C_e, C_t = initial equilibrium and adsorbate concentrations after time t.

3. Results and Discussion

3.1. Characterization

3.1.1. Analysis of the UV-Visible Spectrum. The use of UV-visible spectrum analysis to confirm HAp NP synthesis was investigated. The spectral properties of Ca metal are related to a prominent peak in the UV-visible spectrum between 200 and 220 nm as shown in Figure 1. Due to the encapsulation by the polymer in the leaf extract, the pick corresponds to the surface Plasmon resonance (vibrations) of HAp NPs, and it is the hallmark signal for HAp NPs. This finding is quite similar to those of prior investigations [26]. There were no other peaks in the spectrum, showing that the HAp NPs synthesized by this rapid and green approach were of significant purity.

3.1.2. FT-IR Analysis. FT-IR spectroscopic analysis revealed the presence of phytochemicals that acted as capping agents for the synthesis and stabilization, like phenols, amines, ether, and carboxylic acids, and also used to evaluate the functional groups in HAp NPs [27]. Figure 2(a) represents the spectrum of *M. longifolium* leaf extract. The spectrum shows peaks at 3457, 2088, and 1627 cm^{-1}. The strong and broader band at 3457 cm^{-1} indicates -OH functional groups available in alcohols and phenolic substances contained in the plant extract. The C-N stretching of the cyanide group is represented by the absorption peak at 2088 cm^{-1}. The presence of aldehydes, ketones, and esters is indicated by absorptions in the complex range, i.e., from 1600 to 1760 cm^{-1}, and corresponds to the C=O stretching [28, 29].

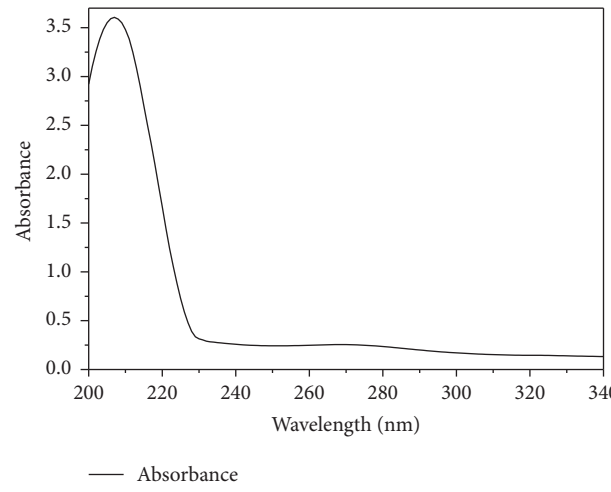

Figure 1: UV-Vis absorption spectrum of HAp NPs synthesized using aqueous extract of *M. longifolium* leaf at room temperature.

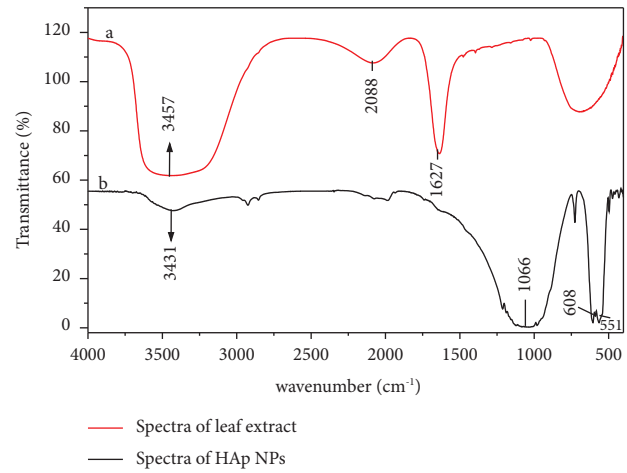

Figure 2: (a) FT-IR spectrum of the aqueous extract of *M. longifolium* leaf and (b) HAp NPs.

The FT-IR spectrum of the HAp NPs is presented in Figure 2, and it has peaked at 3431, 1066, 608, and 551 cm^{-1}. The strong peak at 3431 cm^{-1} corresponds to the characteristic stretching hydroid group [30]. The formation of HAp NPs is confirmed by absorption peaks at 551, 608, and 1066 cm^{-1}. The absorption peaks at 551, 608, and 1066 cm^{-1} prove the synthesis of HAp NPs, and the peaks at 608 and 551 cm^{-1} correspond to the bending vibrations of O-P-O in the phosphate group PO_4^{3-} [31]. The results of this investigation are in accordance with those of Zhang and Poinern et al. [32].

3.1.3. Powder XRD Analysis. X-ray diffraction (XRD) is a versatile, nondestructive analytical method for identification and quantitative determination of various crystalline forms present in powder and solid samples [33]. The XRD pattern of sensitized HAp NPs powder is shown in Figure 3. This pattern shows a series of diffraction peaks in the whole spectra of 2θ values ranging from 26 to 49° (Figure 3). The

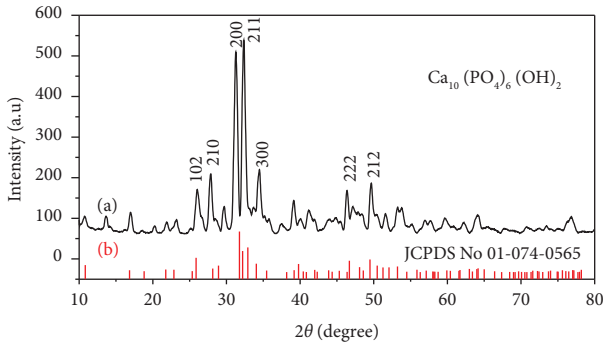

Figure 3: (a) XRD pattern of synthesized HAp NPs and (b) standard diffraction angle.

distinct diffraction peaks at 26.07°, 27.85°, 31.28°, 32.34°, 34.43°, 46.37°, and 49.63° correspond to (102), (210), (200), (211), (300), (222), and (212) miller planes, respectively. This confirms the crystalline structure of the HAp NPs produced, and a similar finding was reported by Sonmez et al. [33].

A typical XRD pattern of the synthesized HAp NPs is compared with the standard values of JCPDS file no. 01-074-0565. All possible peaks can be indexed to the pure hexagonal phase of HAp NPs (P63mc). This confirmed the successful formation of HAp NPs. Furthermore, the green-synthesized HAp NPs have an average crystallite size of 13.17 nm, and Debye–Scherrer's equation was used to identify the nano-sized structure of the composite particle formed (equation (3)).

$$D = \frac{K\lambda}{\beta \cos\theta}, \tag{3}$$

where CuK is the irradiation wavelength; D is the crystalline domain's mean particle size; β = full width at half-maximum (FWHM) of the diffraction peak in radian; and θ = Bragg's diffraction angle crossbanding to the miller indices (211) plane.

3.1.4. Surface Morphology. The morphological structure of the prepared nanocomposite was revealed in SEM. These analyses are useful in the establishment of crystalline structure, chemical composition, and crystal orientations. Figure 4 shows the SEM images of the synthesized HAp NPs at various magnification levels (X1500, X3500, X700, and X10000).

It was observed from the surface morphology of the synthesized HAp NPs that it is hexagonal. It can also be seen from the micrograph that the material is homogeneous and bigger particles are formed by the agglomeration of smaller ones which might be due to the interactions and van der Waals forces existing among HAp NPs [34]. The particle size distribution of NPs was evaluated using ImageJ software, which treated the NPs as spheres and accordingly calculated the size distribution from the deduced area. It was discovered that the majority of the particles are in the 10–50 nm range (Figure 5).

Determination of pHpzc. Point-of-zero charge (pHpzc) was determined using the method described in [35]. Accordingly, pH 7.70 was found to be a pHpzc (Figure 6). The pH values of the adsorbents fall in the acidic to the slightly neutral region. Under pHpzc, the adsorbents' net surface charge is positive, while above pHpzc, it is negative. Thus, determining the pHpzc value aids in determining the appropriate pH level for adsorption studies. To create a predominantly positive charged surface, the pH values should be kept below 7.70 [36, 37].

3.2. Adsorption Study

3.2.1. Effect of Solution pH. The pH of a solution affects the surface charge of adsorbents as well as the degree of ionization of some pollutants. The adsorption of other ions is also influenced by the pH of the solution because the hydrogen ion and hydroxyl ions are effectively adsorbed [38]. In acidic conditions, OH^- groups of HAp NPs can interact with H^+ in solution to form positively charged surfaces [39]. In alkali condition, OH^- ions competing for adsorption sites on the adsorbent surface, and fluoride ions, are repelled by the negatively charged adsorbent surface [40].

In the present study, the influence of pH was investigated by changing the value from 1 to 13. When the pH range changed from 1 to 7, both the percentage removal and adsorption capacity rose from 73 to 93% as shown in Figure 7. When pH is increased to 13, the percentage removal and adsorption capacity decreased to 81% and 13.24 mg/g, respectively, showing that the maximum percentage removal occurred at pH 7.0 and that increasing the pH further did not result in any increase in the percentage removal or adsorption capacity of the nanoparticles. To achieve optimum removal efficiency and fluoride ion absorption capacity, neutral pH was chosen as the ideal one. The results of this investigation are in accordance with the study by Mwakabona et al. [41], who found that when pH increased, both removal efficiency and adsorption capacity enhanced gradually until an equilibrium point was reached.

3.2.2. Effect of Adsorbent Dose. The adsorbent dosage is a critical factor that affects both the removal efficiency and cost-effectiveness of the process. The effect of adsorbent dosage was studded by increasing the adsorbent dosage. The increase in the adsorbent dosage enhances the availability of binding sites and leads to a rise in removal efficiency until equilibrium is attained [42]. The adsorption measures the ability of an adsorbent to remove adsorbate from the solution. The adsorbent's surface is made up of sites with a wide variety of binding energies, according to the surface site heterogeneity model. All sorts of sites are completely exposed to adsorbate adsorption at lower doses for such adsorbents, and the surface becomes saturated quickly, resulting in maximum adsorption. However, as the adsorbent dosage increases, the availability of higher energy sites diminishes and a greater fraction of lower energy sites gets filled up, resulting in a drop in adsorption capacity [43].

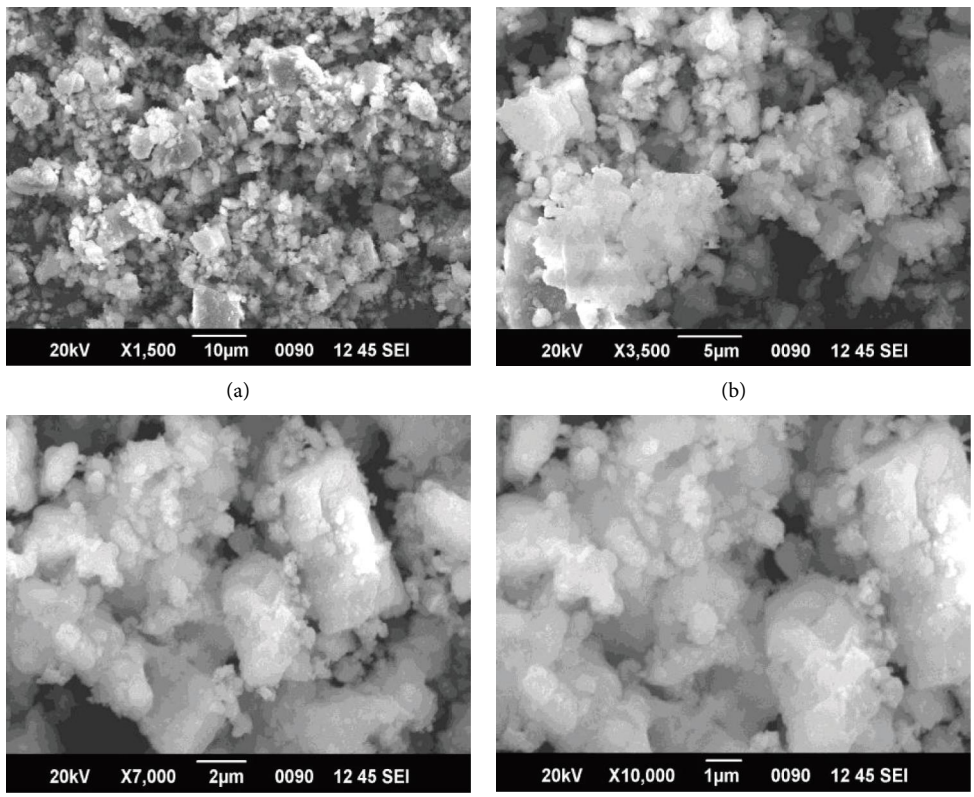

Figure 4: SEM images of the synthesized HAp NPs, at different magnifications.

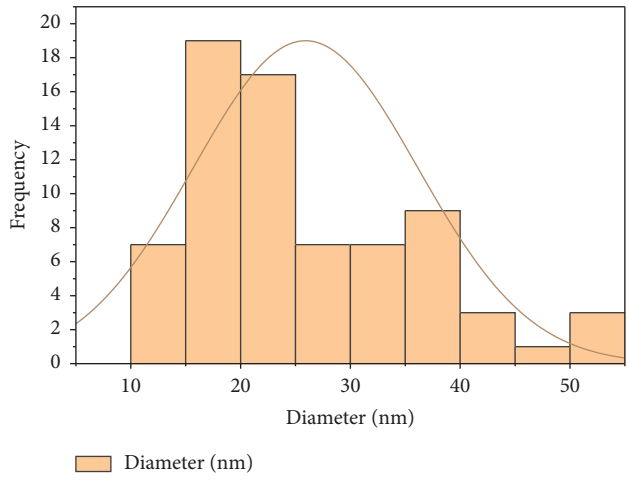

Figure 5: Size distributions of HAp NPs.

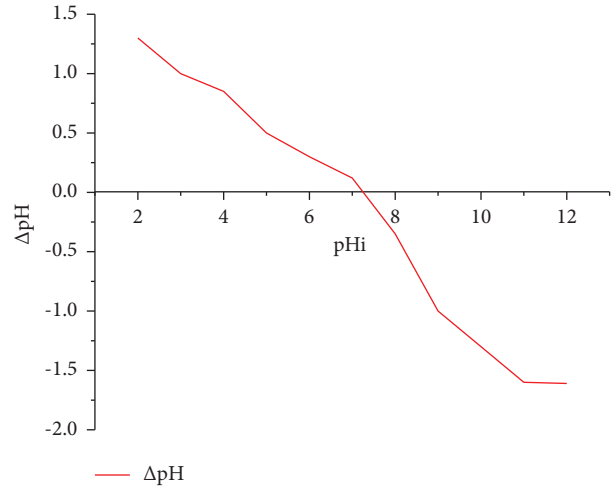

Figure 6: pHpzc for HAp NPs.

In the present study, the percentage removal and adsorption capacity are investigated and illustrated in Figure 8. As observed from the figure, the percentage removal of fluoride ion increases significantly up to an adsorbent dose of 0.75 g/L; however, no significant change was observed when the adsorbent dosage beyond 0.75 g/L rather than the increase in the amount of sludge and the adsorption capacity diminishes with increasing dose. The increase in removal efficiency with increase of adsorbent dose is due to the increase in the availability of binding sites. As a result, 0.75 g of adsorbent was discovered to be the best optimum dosage and this result has better matching with some of the previous research work [44, 45].

Effect of Contact Time. The effects of contact time on the adsorption process were investigated to determine how long it took to attain the equilibrium; HAp NPs were used to remove fluoride ions from an aqueous solution at an

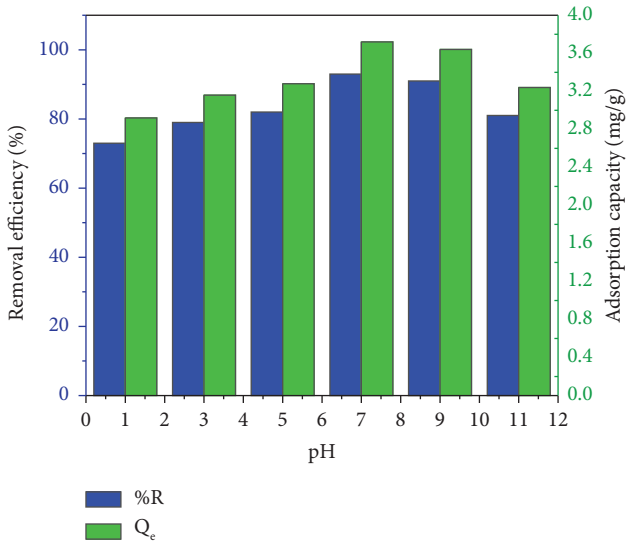

Figure 7: Effect of pH on fluoride ion % removal and equilibrium adsorption capacity (0.25 g adsorbent, 30 min contact time, 10 mg starting fluoride concentration, and 25°C).

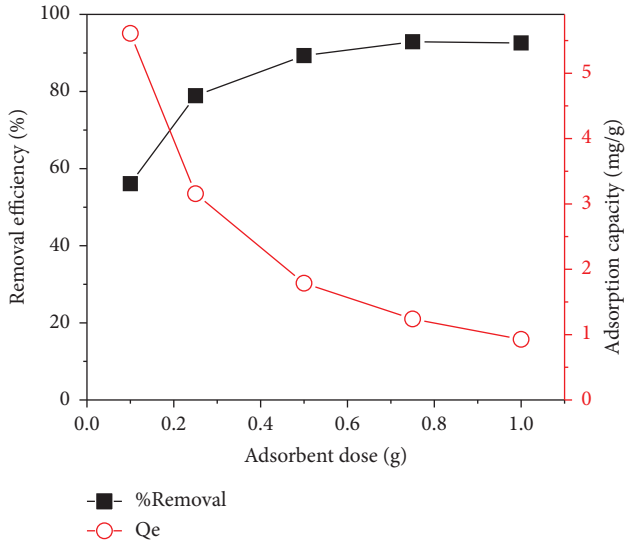

Figure 8: Effect of adsorbent dose on removal efficiency and equilibrium adsorption capacity (pH = 7, 30 min contact time, 10 mg/L starting fluoride ion concentration at 25°C).

optimal pH, adsorbent dosage, and initial fluoride ion concentrations.

The experimental results reveal (Figure 9) that during the first stage of adsorption, both the removal efficiency and adsorption capacity of the adsorbent (HAp NPs) considerably increased and then proceeded at a slower rate with the contact time until a condition of equilibrium was attained. It is possible to explain this phenomenon by the fact that there are many vacant/empty surface sites available for adsorption initially, but as time passes, the remaining vacant surface sites became difficult to be filled and the process slows down due to the repulsive forces between the solute molecules in the solid and bulk phases [46]. The percentage removal and

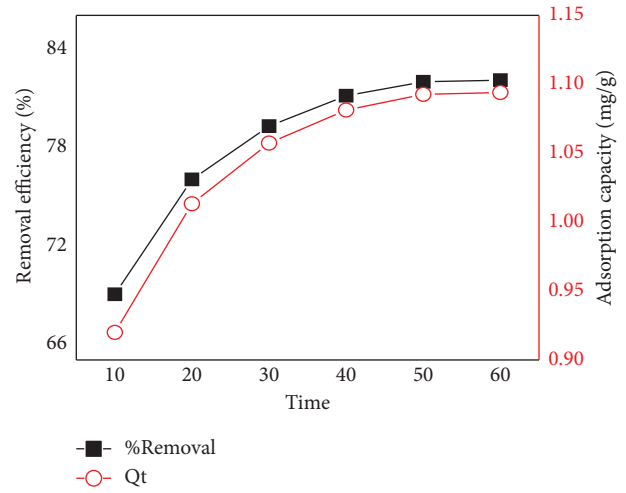

Figure 9: Adsorption capacity and removal efficiency of HAp NP as a function of contact time.

adsorption capacity did not increase as contact duration was increased. Higher removal efficiency (82%) and adsorption capacity (1.09 mg/g) were observed at 50 min; hence, 50 min was considered as the equilibrium time.

3.2.3. Effect of Initial Fluoride Ion Concentrations. By adjusting the starting fluoride ion concentrations from 2.5 to 20 mg/L and using the optimal value of other parameters, the effect of initial fluoride ion concentrations on the adsorption capacity and percentage removal rate by HAp NPs was investigated. Figure 10 indicates that the removal efficiency decreases from 96 to 73.3% when the initial concentration increased from 2.5 to 20 mg/L. The reason for this could be that the ratio of the initial number of fluoride ions to the number of active sites is minimal at lower initial concentrations, resulting in higher removal efficiency; however, the total number of possible adsorption sites for a fixed adsorbent dosage was constant which become saturated at higher concentrations. As a result, after reaching equilibrium, enhancement in the initial concentration did not result in a substantial increase in F-removal efficiency or adsorption capacity but merely result in some residual fluoride ions in the aqueous solution. Therefore, the optimum initial fluoride ion concentration observed was 15 mg. A similar result was reported for fluoride ion removal by the binary code system, aluminum-manganese oxide composite [35].

3.2.4. Effect of Solution Temperature on Adsorption. The solution temperature affects the adsorption process in two ways. Firstly, enhancing the temperature is known to increase the rate of diffusion of adsorbate molecules through the external boundary and interior pores of the adsorbent, because of a decrease in the viscosity of the solution. The second point is that temperature has an effect on the equilibrium capacity of the adsorbent for a given adsorbate. By fixing the optimum value of other parameters, the influence of solution temperature on the adsorption process

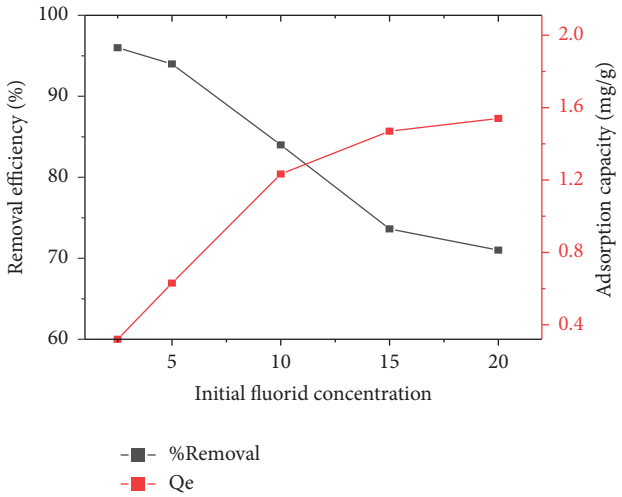

Figure 10: The effect of initial fluoride ion concentration on the removal efficiency and adsorption capacity.

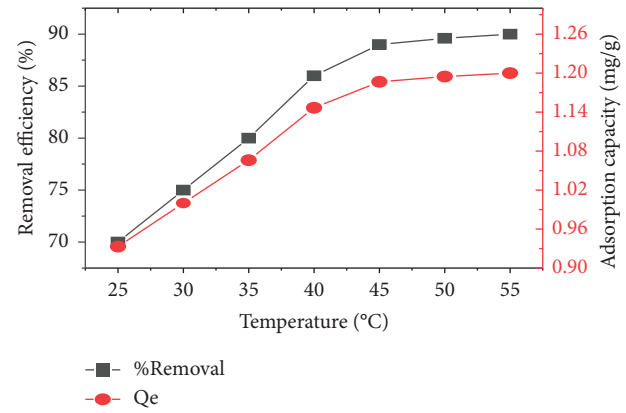

Figure 11: The influence of solution temperature on fluoride ion removal percentage and adsorption capacity.

was investigated at different temperatures: 25, 30, 35, 40, 45, 50, and 45°C.

The data presented in Figure 11 show the adsorption of the fluoride ions by HAp NPs. With a temperature increase from 25 to 45°C, the percentage elimination went from 70 to 90%. Similarly, as the temperature rises from 25 to 45°C, the adsorption capabilities of HAp NPs rose from 0.466 to 0.593 mg/g. The enhancement in percentage removal with temperature is due to the movement of the solute [47]. At a higher temperature, the effective intraparticle diffusion of adsorbate molecules into the pores of the adsorbent occurs. This could be attributed to stronger chemical interaction between the adsorbate and the adsorbent or the development of newer adsorption sites. Siddiqui et al. found a similar result in their investigation on the adsorption of lead (II), cobalt (II), and iron (II) from an aqueous solution by activated carbon [48].

3.3. Adsorption Isotherm. To use adsorbents as efficiently as possible, the adsorption isotherm, which describes how the adsorbate interacts with the adsorbent, is optimized. It is necessary to establish a relationship between a sorption-sorbate system and equilibrium data to remove fluoride ions from the liquid phase. For both linear and nonlinear analysis, the two most popular adsorption isotherm models (Langmuir and Freundlich) were investigated.

3.3.1. Linear Isotherm Analysis. One of the most effective methods for quantifying the distribution of adsorbates, quantitatively assessing adsorption systems, and confirming the theoretical premises of a particular model has been linear regression [49]. Therefore, the accuracy of an adsorption model's fit to experimental data is often evaluated based on the magnitude of the linear coefficient of determination, with R^2 values closest to unity being judged to give the best fit. Accordingly, linear regression of both the Freundlich and Langmuir model parameters was calculated and is presented in Table 1.

The findings from the linear adsorption isotherm analyses are shown in Figure 12 and Table 1. R^2 values of the Langmuir isotherm (0.994) were lower than those of the Freundlich isotherm (0.999) as shown in Figure 12 and Table 1. This suggests that the Freundlich isotherm model fits fluoride sorption onto HAp NPs better. The fact that the Freundlich isotherm model fits the events may be attributed to the creation of multilayer sorbed fluoride ions due to a stronger chemical contact than a physical link. The findings of the current study are in agreement with some of the earlier results [50].

3.3.2. Nonlinear Isotherm Analysis. Using the original form equation (Table 2), nonlinear optimization provides a rigorous mathematical method for figuring out the adsorption model's parameters. However, to evaluate how well a model fits experimental adsorption data, an error function must be chosen [51]. As a result, the various types of mistakes were normalized before choosing the model's parameters whose error function accounted for the minimal sum of normalized errors, indicating the best overall fit [52].

The findings demonstrate that the Freundlich model has a very high coefficient of determination ($R^2 > 0.99$) and extremely low values of the error functions (X^2), better describing the phenomenon of HAp NPs adsorption. This is further supported by observing the nonlinear plot between the experimental data and the models as shown in Figure 13. This is based on the hypothesis that the adsorbent surface is heterogeneous and that the heat of adsorption is distributed unevenly throughout the surface, indicating multilayer adsorption [53].

To choose the best form for an adsorption study, linear and nonlinear approaches to each adsorption isotherm were compared. In the majority of circumstances, the linear version of the Freundlich adsorption isotherm was found to be preferable to the nonlinear form with small error functions.

3.4. Adsorption Kinetics. Kinetic studies are especially important in designing treatment systems whose effectiveness depends on the rate at which fluoride removal

Table 1: Linear sorption isotherm model equation and parameter data.

Isotherm model	Equation	Parameter	CV
Langmuir	$(1)/(q_e) = (1)/(q_{m^b}) * (1)/(C_e) + (1)/(q_e)$	q_m	1.87
		K_L	9.34
		R_L	0.011
		R^2	0.994
		K_F	1.65
		$1/n$	0.84
Freundlich	$\log q_e = \log K_F + (1)/(n) \log C_e$	R^2	0.999

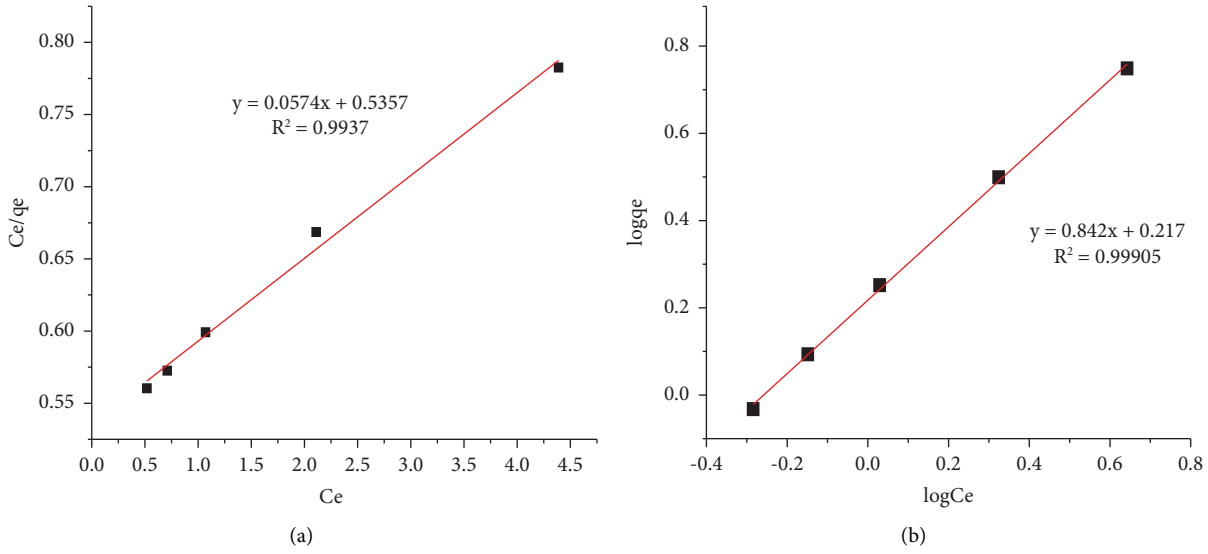

Figure 12: Isotherms models of (a) Langmuir and (b) Freundlich for the adsorption of fluoride onto HAp NPs.

Table 2: Nonlinear sorption isotherm model equation, parameter, and error function data.

Isotherm model	Equation	Parameter	CV
Langmuir	$q_e = (Q_{\max} K_L C_e)/(1 + K_L C_e)$	$Q_{\max}$ (mg g)	7.578
		K_L	0.124
		R^2	0.993
		X^2	0.007
Freundlich	$q_e = K_F C^{1/n}$	K_F	0.863
		N	0.776
		R^2	0.998
		X^2	$7.76E-04$

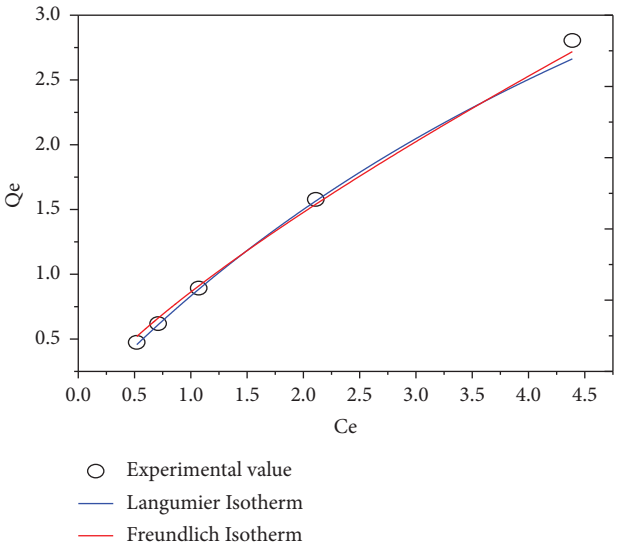

Figure 13: Nonlinear regression of adsorption isotherm models.

occurs. In the current work, linear and nonlinear pseudo-first- and second-order kinetics were used to conduct a kinetic investigation for fluoride adsorption at various time intervals.

3.4.1. Linear Kinetic Models. Batch adsorption tests with 0.75 g HAp NPs in 15 mL of fluoride ion solution were performed for the linear kinetic model analyses. The kinetic parameters obtained from both the first-order and second-order models are shown in Table 3 and Figure 14. Both theories fit the experimental data well in this case. A greater correlation coefficient (R^2) value was however obtained from the pseudo-second-order (0.999) kinetic model, whereas that obtained from the pseudo-first-order kinetic model was lower (0.934), suggesting that chemisorption is the dominant rate-determining process [54].

Table 3: Linear kinetic model equation and calculated parameter value.

Kinetic models	Equation	Parameter	CV
PFO	$\log(q_e - q_t) = \log q_e - (k1)/(2.303)\,t$	K_1	−0.0012
		qe	1.06
		R^2	0.93
PSO	$(1)/(q_e) - q_t = (1)/(q_e) - k_1 t$	K_2	0.624
		qe	1.14
		qe^2	1.3
		R^2	0.999

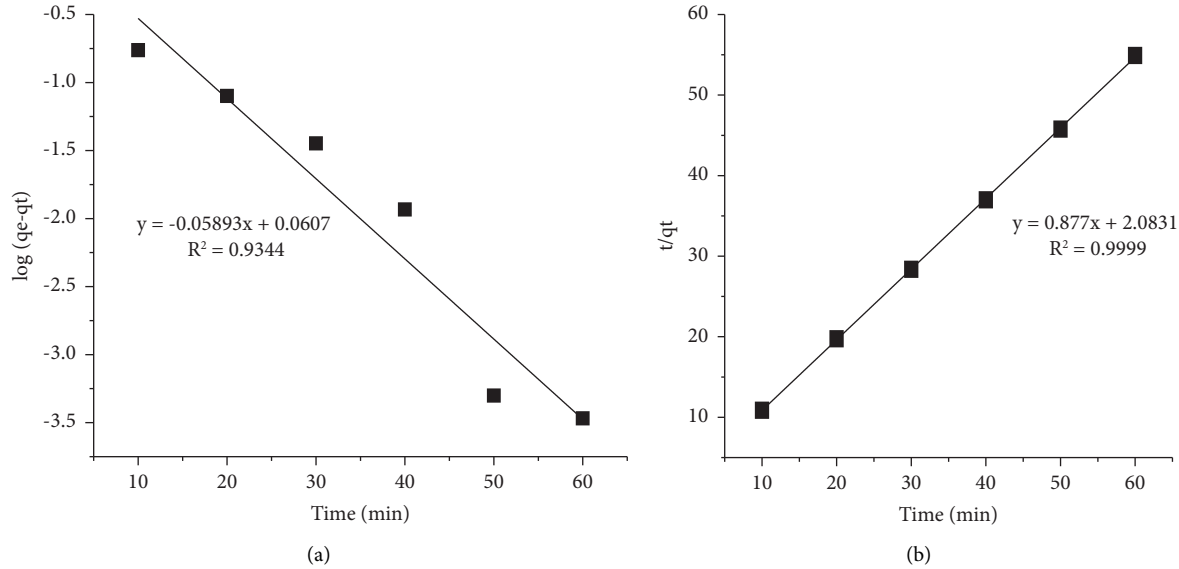

Figure 14: (a) Pseudo-first-order and (b) pseudo-second-order kinetic models for fluoride ion adsorption on HAp NPs.

3.4.2. Nonlinear Kinetic Models. The number of parameters in the nonlinear equation has a significant impact on the goodness of the data fit for nonlinear kinetic models [55]. As a result, nonlinear regression was used to estimate the parameters of the pseudo-first-order and pseudo-second-orderkinetic models. The obtained kinetic parameters and error function data are shown in Table 4 and Figure 15. Accordingly, compared to the pseudo-first-order kinetic equation, the pseudo-second-order kinetic equation has a larger R^2 value and a lower X^2 value. This exhibit of pseudo-second-order kinetics has a good correlation with the experimental data, and the adsorption process predominantly followed the pseudo-second-order kinetic model. This suggests that chemisorption may occur on the surface of an adsorbent simultaneously as a layer of molecules.

3.5. Adsorption Thermodynamics. Equations (4) and (5) were used to calculate the free energy change (ΔG), enthalpy change (ΔH), and entropy change (ΔS) associated with the adsorption process.

$$\Delta G^{\circ} = -\mathrm{RT}\ln \mathrm{Ka}, \tag{4}$$

$$\ln K_a = \left(\frac{\Delta S^{\circ}}{R}\right) - \left(\frac{\Delta H^{\circ}}{\mathrm{RT}}\right). \tag{5}$$

Table 4: Nonlinear kinetic model equation and calculated parameter value.

Kinetic models	Equation	Parameter	CV
PFO	$q_t = q_e(1 - e^{-K_2 t})$	K_1	0.69
		qe	0.571
		R^2	0.8899
PSO	$q_t = (q_e{}^2 K_2 t)/(1 + q_e K_2 t)$	K_2	0.162
		qe	0.675
		R^2	0.988

R is the universal gas constant (0.008314 kJ/mol·K), T is the absolute temperature (K), and Ka is the adsorption equilibrium constant. The Ka values can be calculated by performing adsorption experiments at various temperatures and using equation (4); ΔH^0 and ΔS^0 can then be estimated using a plot of lnKa vs. $1/T$ as described in equation (5) [56].

The acquired data show that as the temperature increased from 298 to 328 K, the adsorption capacity went up (Figure 16), suggesting that fluoride ion adsorption is endothermic. Table 5 summarizes the obtained Gibbs free energy changes (ΔG°) as well as other parameters. The positive value of ΔH° and ΔS° reveals that when the unpredictability of the system grows, the adsorption process becomes endothermic [57]. Up to 318 K, ΔG° was positive,

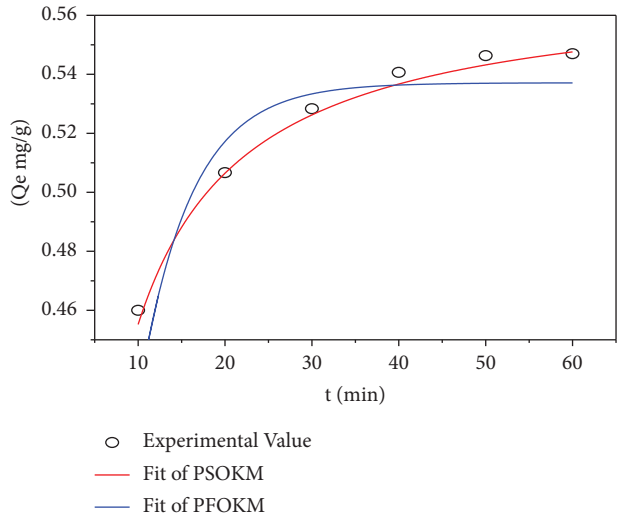

Figure 15: Nonlinear regression of adsorption kinetic models.

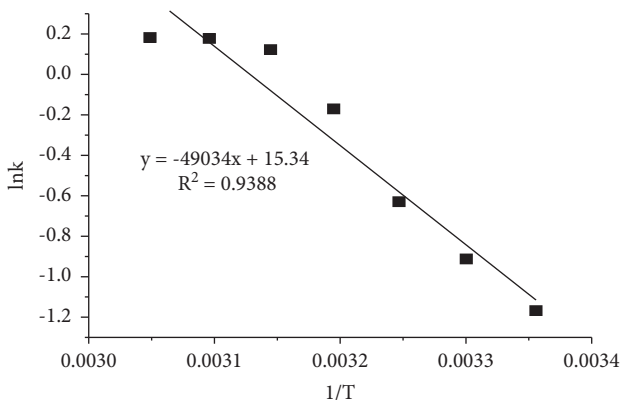

Figure 16: Thermodynamics of the adsorption of fluoride ions onto bone char.

Table 5: Thermodynamic parameters for fluoride ion adsorption on HAp NPs adsorbent.

Adsorbent	Temp (K)	K_L	ΔG° (KJ·mol^{-1})	ΔH° (KJmol^{-1})	ΔS° (JK^{-1}·mol^{-1})	R^2
HAp NPs	298	−1.86	2.89	40.78	127.54	0.94
	303	−1.61	2.30			
	308	−1.33	1.61			
	313	−0.86	0.44			
	318	−0.57	−0.32			
	323	−0.52	−0.48			
	328	−0.51	−0.50			

indicating that the reaction is not spontaneous at lower temperatures (below 318 K), and the values of free energy decrease as temperature rises, indicating that adsorption becomes more spontaneous at higher temperatures. [58]. This phenomenon appears to be in accordance with the kinetic outcome, suggesting that spontaneity is a manifestation of chemical interaction.

3.6. Regeneration of the Adsorbent. Regeneration of used HAp NPs was carried out to validate the reusability. The fluoride ion desorption from exhausted HAp NPs was thus studied (Figure 17). It was done by 40 minutes of shaking the adsorbent in an extract of 0.1 N HCl solutions. Filtration was used to separate the particles, which were then rinsed many times with ultrapure water to eliminate the HCl and

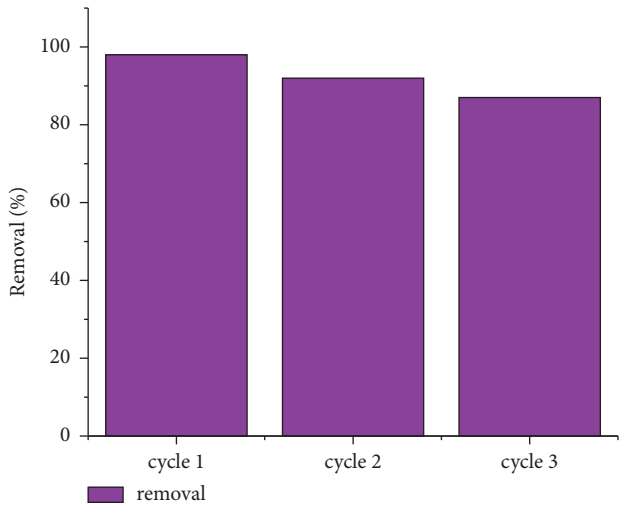

Figure 17: Recycling efficiency of HAp NPs on fluoride removal.

desorbed components. Finally, the HAp NPs that had been regenerated was used three times for fluoride ion adsorption at optimal circumstances.

4. Conclusion

For the adsorptive elimination of fluoride ions from an aqueous solution, HAp NPs were successfully prepared using a green synthesis approach. The synthesized HAp NPs were characterized by UV-Vis, AAS FT-IR, XRD, TGA/DTA, and SEM particularly, to investigate the shape, structure particle size, crystallinity, and functional group. Adsorption was studied as a function of pH, contact time, adsorbent dosage, initial fluoride ion concentration, and solution temperature using the batch method. The results showed that increasing the adsorbent dosage and contact time until the optimum results are achieved resulted in enhanced fluoride ion adsorption, while increasing the amount of initial fluoride ion concentration resulted in decreased adsorption. pH of 7, adsorbent dose of 0.75 g, contact period of 40 min, starting fluoride ion concentration of 10 mg/L, and temperature of 40°C were known to be the optimum adsorption conditions.

The pseudo-second-order, Freundlich model, and the spontaneity of the process best fit the fluoride ion adhesion onto HAp NPs, according to a survey of kinetics, equilibrium isotherm, and thermodynamic research. According to the regeneration test, the tired HAp NPs had similar removal efficacy as the new ones. Thus, HAp NPs made using *M. longifolium* leaf extract is recommended as a quick, effective, and inexpensive adsorbent for removing fluoride ion from an aqueous solution. The present findings suggest that the efficacy of synthesized HAp NPs in the removal of other pollutants (metals, anions, or colors) in wastewater should be studied. Furthermore, other adsorption equilibrium and kinetic models such as the Temkin, intraparticle diffusion, pore diffusion, and Evolich models should be tested on the adsorption data to get more insights into the mechanism of adsorption involved.

Data Availability

The datasets collected and analyzed during the current study are available from the corresponding author upon request; the corresponding author had full access to all the data in the study and takes responsibility for the integrity of the data and the accuracy of the data analysis.

Conflicts of Interest

The authors declare that there are no conflicts of interest.

References

[1] M. E. Kaseva, "Optimization of regenerated bone char for fluoride removal in drinking water: a case study in Tanzania," *Journal of Water and Health*, vol. 4, no. 1, pp. 139–147, 2006.

[2] M. Arif, J. Hussain, I. Husain, and S. Kumar, "Fluoride toxicity and its distribution in groundwater of south east part of Nagaur district, Rajasthan, India," *International Journal of Scientific Research in Agricultural Sciences*, vol. 1, no. 6, pp. 110–117, 2014.

[3] A. Salifu, *Fluoride Removal from Groundwater by Adsorption Technology*, CRC Press, Boca Raton, 2017.

[4] K. Parashar, N. Ballav, S. Debnath, K. Pillay, and A. Maity, "Rapid and efficient removal of fluoride ions from aqueous solution using a polypyrrole coated hydrous tin oxide nanocomposite," *Journal of Colloid and Interface Science*, vol. 476, pp. 103–118, 2016.

[5] S. Jagtap, M. K. Yenkie, N. Labhsetwar, and S. Rayalu, "Fluoride in drinking water and defluoridation of water," *Chemical Reviews*, vol. 112, no. 4, pp. 2454–2466, 2012.

[6] M. Habuda-Stanić, M. E. Ravančić, and A. Flanagan, "A review on adsorption of fluoride from aqueous solution," *Materials*, vol. 7, no. 9, pp. 6317–6366, 2014.

[7] M. Jiménez-Reyes and M. Solache-Ríos, "Sorption behavior of fluoride ions from aqueous solutions by hydroxyapatite," *Journal of Hazardous Materials*, vol. 180, no. 1-3, pp. 297–302, 2010.

[8] X. Fan, D. J. Parker, and M. D. Smith, "Adsorption kinetics of fluoride on low cost materials," *Water Research*, vol. 37, no. 20, pp. 4929–4937, 2003.

[9] N. S. Yapo, S. Aw, B. G. H. Briton, P. Drogui, K. B. Yao, and K. Adouby, "Removal of fluoride in groundwater by adsorption using hydroxyapatite modified Corbula trigona shell powder," *Chemical Engineering Journal Advances*, vol. 12, Article ID 100386, 2022.

[10] V. Sternitzke, R. Kaegi, J. N. Audinot, E. Lewin, J. G. Hering, and C. A. Johnson, "Uptake of fluoride from aqueous solution on nano-sized hydroxyapatite: examination of a fluoridated surface layer," *Environmental Science & Technology*, vol. 46, no. 2, pp. 802–809, 2012.

[11] S. Pokhrel, "Hydroxyapatite: preparation, properties and its biomedical applications," *Advances in Chemical Engineering and Science*, vol. 08, no. 4, pp. 225–240, 2018.

[12] M. Sundrarajan, S. Jegatheeswaran, S. Selvam, N. Sanjeevi, and M. Balaji, "The ionic liquid assisted green synthesis of hydroxyapatite nanoplates by Moringa oleifera flower extract: a biomimetic approach," *Materials & Design*, vol. 88, pp. 1183–1190, 2015.

[13] M. I. Kay, R. A. Young, and A. S. Posner, "Crystal structure of hydroxyapatite," *Nature*, vol. 204, no. 4963, pp. 1050–1052, 1964.

[14] A. Corami, S. Mignardi, and V. Ferrini, "Cadmium removal from single- and multi-metal solutions by sorption on hydroxyapatite," *Journal of Colloid and Interface Science*, vol. 317, no. 2, pp. 402–408, 2008.

[15] M. Islam, P. Chandra Mishra, and R. Patel, "Physicochemical characterization of hydroxyapatite and its application towards removal of nitrate from water," *Journal of Environmental Management*, vol. 91, no. 9, pp. 1883–1891, 2010.

[16] T. G. P. Galindo, Y. Chai, and M. Tagaya, "Hydroxyapatite nanoparticle coating on polymer for constructing effective biointeractive interfaces," *Journal of Nanomaterials*, vol. 2019, Article ID 6495239, 23 pages, 2019.

[17] A. Mushtaq, R. Zhao, D. Luo et al., "Magnetic hydroxyapatite nanocomposites: the advances from synthesis to biomedical applications," *Materials & Design*, vol. 197, Article ID 109269, 2021.

[18] N. Mohd Pu'ad, P. Koshy, H. Z. Abdullah, M. I. Idris, and T. C. Lee, "Syntheses of hydroxyapatite from natural sources," *Heliyon*, vol. 5, no. 5, Article ID e01588, 2019.

[19] C. Ragunath, L. Kousalya, R. Venkatachalam, and S. Anitha, "Green synthesis of hydroxyapatite nanoparticles from wrightia tinctoria and its antibacterial activity," *BioNanoScience*, vol. 12, no. 3, pp. 723–730, 2022.

[20] K. Alorku, M. Manoj, and A. Yuan, "A plant-mediated synthesis of nanostructured hydroxyapatite for biomedical applications: a review," *RSC Advances*, vol. 10, no. 67, pp. 40923–40939, 2020.

[21] A. Zenebe, A. M. Yimer, A. Mohammed Yimer, S. Kuzhunellil, and H. Demissie, "Green synthesis of magnetic nanocomposite by leave extract for the treatment of Methylene blue contaminated water," *Chemical Engineering Journal Advances*, vol. 8, Article ID 100193, 2021.

[22] E. Nyankson, J. Adjasoo, J. K. Efavi et al., "Characterization and evaluation of zeolite A/Fe3O4 nanocomposite as a potential adsorbent for removal of organic molecules from wastewater," *Journal of Chemistry*, vol. 2019, Article ID 8090756, 13 pages, 2019.

[23] P. Vishnukumar, S. Vivekanandhan, M. Misra, and A. K. Mohanty, "Recent advances and emerging opportunities in phytochemical synthesis of ZnO nanostructures," *Materials Science in Semiconductor Processing*, vol. 80, pp. 143–161, 2018.

[24] V. Kalaiselvi, R. Mathammal, N. Vidhya, and K. Surya, "Synthesis and characterization of pure and capped hydroxyapatite nanoparticles," *International Journal of Advanced Science and Engineering*, vol. 6, no. 1, pp. 1213–1219, 2019.

[25] V. Kalaiselvi, R. Mathammal, S. Vijayakumar, and B. Vaseeharan, "Microwave assisted green synthesis of Hydroxyapatite nanorods using Moringa oleifera flower extract and its antimicrobial applications," *International journal of veterinary science and medicine*, vol. 6, no. 2, pp. 286–295, 2018.

[26] T. S. de Araujo, S. O. De Souza, and E. M. B. De Sousa, "Effect of Zn2+, Fe3+ and Cr3+ addition to hydroxyapatite for its application as an active constituent of sunscreens," *Journal of Physics: Conference Series*, vol. 249, Article ID 012012, 2010.

[27] V. Veeramanikandan, G. Madhu, V. Pavithra, K. Jaianand, and P. Balaji, "Green synthesis, characterization of iron oxide nanoparticles using leucas aspera leaf extract and evaluation of antibacterial and antioxidant studies," *International Journal of Agriculture Innovations and Research*, vol. 6, pp. 242–250, 2017.

[28] L. Liu, J. Cao, J. Huang, Y. Cai, and J. Yao, "Extraction of pectins with different degrees of esterification from mulberry branch bark," *Bioresource Technology*, vol. 101, no. 9, pp. 3268–3273, 2010.

[29] S. Alayande, T. Adeseluka, B. Odewumi et al., "Evaluation of Microbial Inhibition Properties of Green and Chemically Synthesized ZnO Nanoparticles," *Bulletin of Materials Science*, vol. 42, 2019.

[30] F. Mohandes and M. Salavati-Niasari, "In vitro comparative study of pure hydroxyapatite nanorods and novel polyethylene glycol/graphene oxide/hydroxyapatite nanocomposite," *Journal of Nanoparticle Research*, vol. 16, no. 9, pp. 2604–2612, 2014.

[31] G. Bharath, B. S. Latha, E. H. Alsharaeh, P. Prakash, and N. Ponpandian, "Enhanced hydroxyapatite nanorods formation on graphene oxide nanocomposite as a potential candidate for protein adsorption, pH controlled release and an effective drug delivery platform for cancer therapy," *Analytical Methods*, vol. 9, no. 2, pp. 240–252, 2017.

[32] G. J. E. Poinern, R. L. X. T. Brundavanam, X. T. Le, S. Djordjevic, M. Prokic, and D. Fawcett, "Thermal and ultrasonic influence in the formation of nanometer scale hydroxyapatite bio-ceramic," *International Journal of Nanomedicine*, vol. 6, pp. 2083–2095, 2011.

[33] E. Sonmez, I. Cacciatore, F. Bakan et al., "Toxicity assessment of hydroxyapatite nanoparticles in rat liver cell model in vitro," *Human & Experimental Toxicology*, vol. 35, no. 10, pp. 1073–1083, 2016.

[34] G. Sharma, R. Soni, and N. D. Jasuja, "Phytoassisted synthesis of MagnesiumOxide nanoparticles with swertia chirayaita," *Journal of Taibah University forScience*, vol. 11, no. 3, pp. 471–477, 2017.

[35] S. Alemu, E. Mulugeta, F. Zewge, and B. S. Chandravanshi, "Water defluoridation by aluminium oxide–manganese oxide composite material," *Environmental Technology*, vol. 35, no. 15, pp. 1893–1903, 2014.

[36] K. Parashar, N. Ballav, S. Debnath, K. Pillay, and A. Maity, "Hydrous ZrO2 decorated polyaniline nanofibres: synthesis, characterization and application as an efficient adsorbent for water defluoridation," *Journal of Colloid and Interface Science*, vol. 508, pp. 342–358, 2017.

[37] A. A. Izuagie, W. M. Gitari, and J. R. Gumbo, "Synthesis and performance evaluation of Al/Fe oxide coated diatomaceous

earth in groundwater defluoridation: towards fluorosis mitigation," *Journal of Environmental Science and Health, Part A*, vol. 51, no. 10, pp. 810–824, 2016.

[38] W. Shen, Z. Li, and Y. Liu, "Surface chemical functional groups modification of porous carbon," *Recent Patents on Chemical Engineering*, vol. 1, pp. 27–40, 2008.

[39] A. A. El Hadad, E. Peón, F. García-Galván et al., "Biocompatibility and corrosion protection behaviour of hydroxyapatite sol-gel-derived coatings on Ti6Al4V alloy," *Materials*, vol. 10, no. 2, p. 94, 2017.

[40] T. Akafu, A. Chimdi, and K. Gomoro, "Removal of fluoride from drinking water by sorption using diatomite modified with aluminum hydroxide," *Journal of analytical methods in chemistry*, vol. 2019, Article ID 4831926, 11 pages, 2019.

[41] H. T. Mwakabona, R. Machunda, and K. N. Njau, "The Influence of Stereochemistry of the Active Compounds on Fluoride Adsorption Efficiency of the Plant Biomass," *American Journal of Chemical Engineering*, vol. 2, no. 4, pp. 42–47, 2014.

[42] A. Chemburkar, A. Sartape, A. Gawade, P. Somawanshi, and J. Ghorpade, "Automated tool for plant leaf classification using morphological features," *International Journal of Engineering and Computer Science*, vol. 3, pp. 9098–9102, 2014.

[43] J. Utsev, R. Iwar, and K. Ifyalem, "Adsorption of methylene blue from aqueous solution onto delonix regia pod activated carbon: batch equilibrium isotherm, kinetic and thermodynamic studies," *Agricultural Wastes*, vol. 4, pp. 18-19, 2020.

[44] W. Nigussie, F. Zewge, and B. S. Chandravanshi, "Removal of excess fluoride from water using waste residue from alum manufacturing process," *Journal of Hazardous Materials*, vol. 147, no. 3, pp. 954–963, 2007.

[45] M. Regassa, F. Melak, W. Birke, and E. Alemayehu, "Defluoridation of water using natural and activated coal," *Int. Adv. Res. J. Sci. Eng. Technol*, vol. 3, pp. 1–7, 2016.

[46] J. Fito, H. Said, S. Feleke, and A. Worku, "Fluoride removal from aqueous solution onto activated carbon of Catha edulis through the adsorption treatment technology," *Environmental Systems Research*, vol. 8, no. 1, 2019.

[47] M. C. Ncibi, B. Mahjoub, and M. Seffen, "Adsorptive removal of textile reactive dye using Posidonia oceanica (L.) fibrous biomass," *International journal of Environmental Science and Technology*, vol. 4, pp. 433–440, 2007.

[48] M. N. Siddiqui, B. Chanbasha, A. Al-Arfaj, T. Kon‟kova, and I. Ali, "Superfast Removal of Cobalt Metal Ions in Water Using Inexpensive Mesoporous Carbon Obtained from Industrial Waste Material," *Environmental Technology & Innovation*, vol. 21, Article ID 101257, 2020.

[49] K. Y. Foo and B. H. Hameed, "Insights into the modeling of adsorption isotherm systems," *Chemical Engineering Journal*, vol. 156, no. 1, pp. 2–10, 2010.

[50] J. P. Maity, C. M. Hsu, T. J. Lin et al., "Removal of fluoride from water through bacterial-surfactin mediated novel hydroxyapatite nanoparticle and its efficiency assessment: adsorption isotherm, adsorption kinetic and adsorption thermodynamics," *Environmental Nanotechnology, Monitoring & Management*, vol. 9, pp. 18–28, 2018.

[51] S. Martinez-Vargas, A. I. Martínez, E. E. Hernández-Beteta et al., "Arsenic adsorption on cobalt and manganese ferrite nanoparticles," *Journal of Materials Science*, vol. 52, no. 11, pp. 6205–6215, 2017.

[52] Y. S. Ho, J. F. Porter, and G. McKay, "Equilibrium isotherm studies for the sorption of divalent metal ions onto peat: copper, nickel and lead single component systems," *Water, Air, and Soil Pollution*, vol. 141, no. 1/4, pp. 1–33, 2002.

[53] A. B. Albadarin and C. Mangwandi, "Mechanisms of Alizarin Red S and Methylene blue biosorption onto olive stone by-product: isotherm study in single and binary systems," *Journal of Environmental Management*, vol. 164, pp. 86–93, 2015.

[54] H. Baseri and S. Tizro, "Treatment of nickel ions from contaminated water by magnetite based nanocomposite adsorbents: effects of thermodynamic and kinetic parameters and modeling with Langmuir and Freundlich isotherms," *Process Safety and Environmental Protection*, vol. 109, pp. 465–477, 2017.

[55] M. I. El-Khaiary and G. F. Malash, "Common data analysis errors in batch adsorption studies," *Hydrometallurgy*, vol. 105, no. 3-4, pp. 314–320, 2011.

[56] A. Sinhababu and A. Banerjee, "Ethno-botanical study of medicinal plants used by tribals of Bankura district West Bengal India," *J Med Plants Stud*, vol. 1, pp. 98–104, 2013.

[57] M. N. Sahmoune, "Evaluation of thermodynamic parameters for adsorption of heavy metals by green adsorbents," *Environmental Chemistry Letters*, vol. 17, no. 2, pp. 697–704, 2019.

[58] Y. Cantu, A. Remes, A. Reyna et al., "Thermodynamics, kinetics, and activation energy studies of the sorption of chromium (III) and chromium (VI) to a Mn3O4 nanomaterial," *Chemical Engineering Journal*, vol. 254, pp. 374–383, 2014.